crystals

MDPI

Article

Study on the Purification Effect and Equilibrium Distribution Coefficient of Impurities during Zone Refining of Fluorene

Yifeng Shang, Jun Li * and Ming Chen

Department of Chemical Engineering, Sichuan University, Chengdu 610065, China
* Correspondence: lijunlab@163.com; Tel./Fax: +86-028-85460936

Abstract: High-purity fluorene is widely used in optoelectronic materials, biology, medicine, and other fields. It is a kind of industrial chemical with high added value. In this paper, zone melting purification technology was used to study the purification effect of fluorene on the zone travel rate, the zone length, the zone passing number, and the zone temperature difference. The concentration distribution of fluorene and the impurities 2-methylbiphenyl, 4-methylbiphenyl, 4-methyldibenzofuran, and dibenzofunan along the moving direction of the melting zone was obtained. A one-pass zone refining model of fluorene was established; the effective distribution coefficients of the four impurities above were obtained via mathematical software fitting; and the equilibrium distribution coefficients were further calculated, which were 0.2441, 0.5850, 0.2377, and 0.3497, respectively. The k_0 of all impurities was less than 1. The purification effect of fluorene can be improved by using a larger zone length in the initial zone melting purification process, a smaller zone travel rate in the whole zone melting purification process, multiple zone melting purification processes, and a larger zone temperature difference. After four zone melting purification processes, the purity of fluorene increased from 97.62% to 99.08%, which was nearly 1.5% higher than the initial purity of fluorene. Zone melting purification technology provides a new idea for the preparation of high-purity fluorene.

Keywords: fluorene; equilibrium distribution coefficient; zone melting purification technology

check for updates

Citation: Shang, Y.; Li, J.; Chen, M. Study on the Purification Effect and Equilibrium Distribution Coefficient of Impurities during Zone Refining of Fluorene. *Crystals* **2023**, *13*, 1224. https://doi.org/10.3390/cryst13081224

Academic Editor: Pedro De Almeida

Received: 27 June 2023
Revised: 1 August 2023
Accepted: 4 August 2023
Published: 9 August 2023

Copyright: © 2023 by the authors. Licensee MDPI, Basel, Switzerland. This article is an open access article distributed under the terms and conditions of the Creative Commons Attribution (CC BY) license (https://creativecommons.org/licenses/by/4.0/).

1. Introduction

Fluorene is an important organic compound. The main structure of a fluorene molecule ($C_{13}H_{10}$) is composed of two benzene rings (Figure 1). The C-C bond and the adjacent methylene bridge link the two benzene rings. Due to the existence of the methylene bridge, the two benzene rings form in the same plane. The degree of orbital overlap and conjugation between them is greatly increased. Because the methylene between the two rings is affected by the benzene ring, the hydrogen atom at position 9 in the fluorene molecule is quite active. Methylene is the chemically active reaction point of fluorene. It can be used to synthesize functional derivatives of fluorene. Fluorene and its derivatives are widely used in fields such as medicine, pesticides, synthetic dyes, engineering plastics, etc. For example, 9, 9-bis-(2-carboxyethyl) fluorene can be used to prepare polyimide resin; 2-dihydroxyaminoacetyl fluorenone can be used as an analgesic and antispasmodic agent; 9-fluorenone-2-carboxy amino alcohol ester can be used as a local anesthetic; 2-dihydroxyaminomethyl fluorene is an antispasmodic, analgesic, and antihypertensive agent; and 5-fluorenoic acid is a plant hormone. Bisphenol fluorene can be used as a raw material of a highly functional polymer. More research and development have focused on fluorene and its derivatives in recent years.

The traditional purification method of fluorene is solvent crystallization. Refined fluorene is prepared via the solvent crystallization of crude fluorene obtained from coal tar rectification. This method can increase the purity of crude fluorene to 97–98% [1]. On the basis of the fluorene obtained, higher purity fluorene can be obtained by repeating solvent crystallization. At present, the differences between the solvent crystallization

methods used to purify fluorene in the literature are the different organic solvents, the different operating parameters of the recrystallization process (cooling speed, stirring intensity, and recrystallization time), and the different washing methods [1–5]. However, too many organic solvents are used, the loss of organic solvents in the crystallization process is inevitable, environmental pollution is serious, and the energy consumption for solvent recovery is also quite high. With purer fluorene that needs to be purified, these shortcomings of the solvent crystallization method become increasingly prominent. Therefore, a new method must be found to prepare high-purity fluorene.

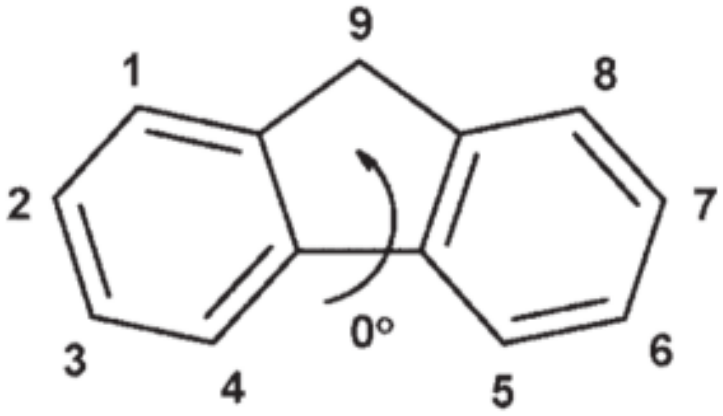


Figure 1. Structure of fluorene molecule.

In order to overcome the shortcomings above, this paper proposes using zone melting technology to purify fluorene. Zone melting uses the different distribution coefficients of impurities in the solid and liquid phases of the purified material to achieve separation. This technology has advantages compared to the solution crystallization method, as it has low energy consumption, is friendly to the environment, requires no solvent, etc. Since Pfann [6] outlined zone melting purification technology in the early 1950s, it has mainly been used in three applications: 1. the preparation of specific crystal forms to meet specific research needs [7–17]; 2. doping substance A into substance B [8,10,11,14–24]; and 3. substance purification. Current research mainly focuses on inorganic substances, such as La [25], Al [26–30], Si [31], Zr [32], Hf [32], Se [33], Te [34–37], Ge [38,39], Sn [40], Cd [41], P [42], 1-ethyl-3-methylimidazole chloride [43], and dibenzyl [44].

The efficiency of zone refining is affected by a variety of experimental factors, which can be altered to optimize the process. These factors include [26,45]:

(1) The effective distribution coefficient (k_{eff}), representing the experimental ratio of C_S to C_L. This factor itself is dependent on the diffusion layer thickness between liquid and solid, the zone travel rate, and the diffusion coefficient of each impurity as well as the heating power.
(2) The zone travel rate, which should normally be kept slow enough to increase the refining efficiency (decrease k_{eff} for $k < 1$ and increase k_{eff} for $k > 1$), but at the same time, a rate that is too low increases the time consumption for each pass tremendously. The term refining efficiency refers to the maximum impurity removal a zone refining process can achieve.
(3) The zone length, which is the length of the molten zone, affecting both the ultimate distribution of the elements and the rate at which it is achieved. This length is affected by many factors, such as the heating power, zone travel rate, thermal conductivity of the crucible and charge, etc.
(4) The zone temperature difference at the solid/liquid interface, influencing the microsegregation of impurities in that area. This is also controlled by the heating power, zone travel rate, thermal conductivity of the crucible and charges, etc.
(5) The zone passing number. Less passes cannot attain a product with high purity; however, more passes consume more time.

Therefore, the zone travel rate, zone length, zone temperature difference, and zone passing number are the four main factors that affect the purification effect of zone melting. This paper studied the influence of these four factors on the purification of fluorene and obtained the equilibrium distribution coefficient of the main impurities in fluorene, which laid the foundation for the subsequent research.

2. Experiment

2.1. Sample

The purity of the fluorene was 97.62% (Table 1). The fluorene was prepared from 77% crude fluorene (industrial product) in the laboratory. The purity was determined using gas chromatography.

Table 1. The contents of each substance in the material after treatment.

Substances	Content (%)
Fluorene	97.6219
2-Methylbiphenyl(D)	0.3146
4-Methylbiphenyl(E)	1.3948
4-Methyldibenzofuran(F)	0.2456
Dibenzofunan(G)	0.1062

2.2. Device

Figure 2 shows the zone melting purification equipment used in the experiment. The equipment was mainly divided into two parts, including a temperature control part and a moving part. The temperature control part consisted of one heating area and two cooling areas, as shown in Figure 3. The heating area and the cooling area were, respectively, composed of a copper heater and a stainless-steel jacket. The lengths of the copper heater and the stainless-steel jacket could be adjusted. The heating area was controlled using a PID temperature controller to adjust the heating power of the copper heater. The temperature of the cooling zone was controlled using water recycled through the jacket. On one hand, the cooling zone limited the extension of the molten zone produced by the heating area. On the other hand, generating crystals from the melt zone using forced cooling achieved the purpose of purification. The moving part consisted of two motors (a high-speed motor and a low-speed motor) and a connecting mechanism.

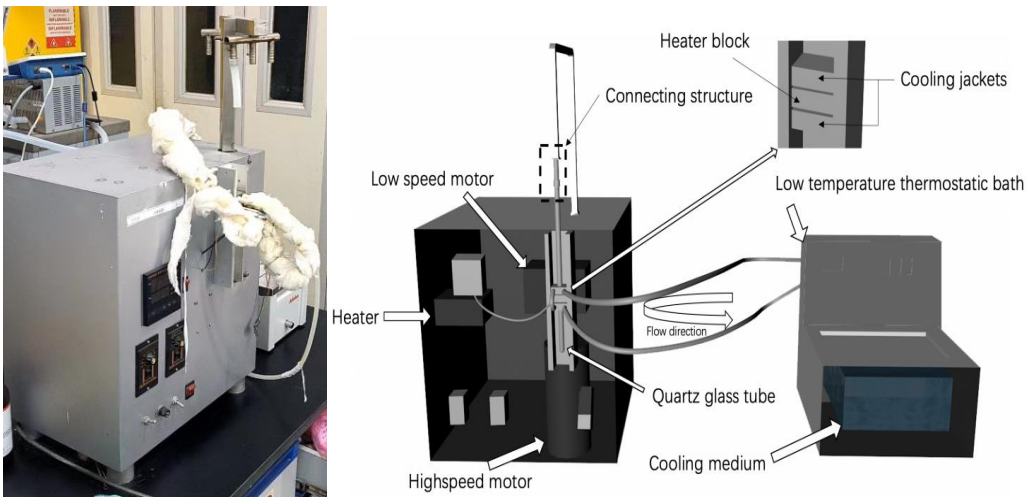


Figure 2. Zone melting equipment.

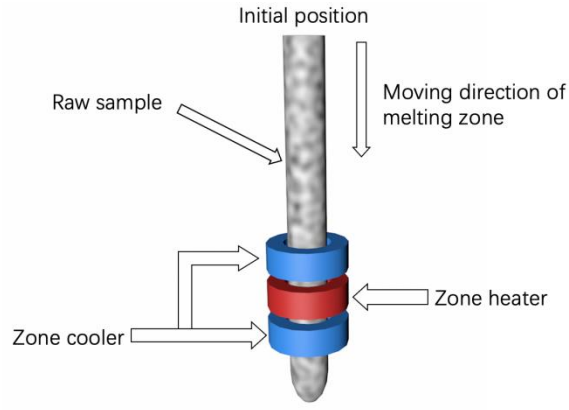


Figure 3. Heating and cooling equipment during zone melting processes.

2.3. Experimental Operation

Sample fluorene was put into a quartz glass tube with a diameter of 12 mm. The tube was sealed. The tube was connected with the zone melting purification equipment via the connecting mechanism. The tube containing the sample fluorene passed through a cooling zone, the heating zone (heating rods inserted into the copper block provided the heat source to melt the fluorene), and a cooling zone (the cooling medium was water) in sequence due to the slow motor at a set speed. When the tube moved to the end, the high-speed motor made the tube reset quickly. Then, repeating the above operation made the fluorene purer. In this process, the control variable method was used to adjust the zone travel rate, zone length, zone temperature difference, and zone passing number for the research.

After the zone melting purification process was completed, the purified fluorene was melted in sections. This process used the Joule heating effect to melt fluorene. Then, the samples were taken out and placed in sampling bottles. Finally, bottles with high-grade pure acetone added were put in a water bath to shake. The samples and acetone were allowed to mix. The analytical instrument was a gas chromatography instrument purchased from Shanghai INESA Analytical Instrument Co., Ltd, Shanghai, China.

2.4. Analytical Methods

The analysis equipment used gas chromatography, and the analysis adopted the area normalization method. The content calculation was carried out as shown in Formula (1), where *Ci* represents the content of substance i and *Ai* represents the chromatographic peak area of substance i.

The chromatographic column was an OV-101 measuring 0.32 mm × 0.25 um × 30 m. The injector temperature was 280 °C. The hydrogen flame ionization detector temperature was 280 °C. The carrier gas was high-purity nitrogen. The starting column temperature was 140 °C. Then, the temperature was increased to 210 °C at the rate of 3 °C/min and then increased to 280 °C at the rate of 10 °C/min. Finally, the column temperature was maintained for 5 min. The types of impurities in the sample fluorene were determined using GC-MS (GCMS-QP2010 Plus, Shimadzu Corporation, Kyoto, Japan). The injector temperature was 290 °C. The starting column temperature was 40 °C, which was maintained for 5 min, then increased to 280 °C at the rate of 10 °C/min. The temperature was maintained for 5 min, then increased to 290 °C at the rate of 5 °C/min, and the temperature was maintained for 10 min. The ion source temperature was 200 °C. The scan speed was 1250, and the ion m/z was scanned from 33 to 600.

$$C_i = \frac{A_i}{\sum A_i} \times 100\% \quad (1)$$

Formula (1): Content calculation formula.

3. Results and Discussion

The comparison of samples before and after zone refining in Figure 4 shows that the pure fluorene was white. It can be clearly seen that the whole material presented a uniform light yellow before zone refining. After several zone refining processes, the sample showed a color change from white to yellow to dark yellow from left to right. Darker yellow represented a higher impurity concentration, indicating that impurities were heavily enriched in the tail.

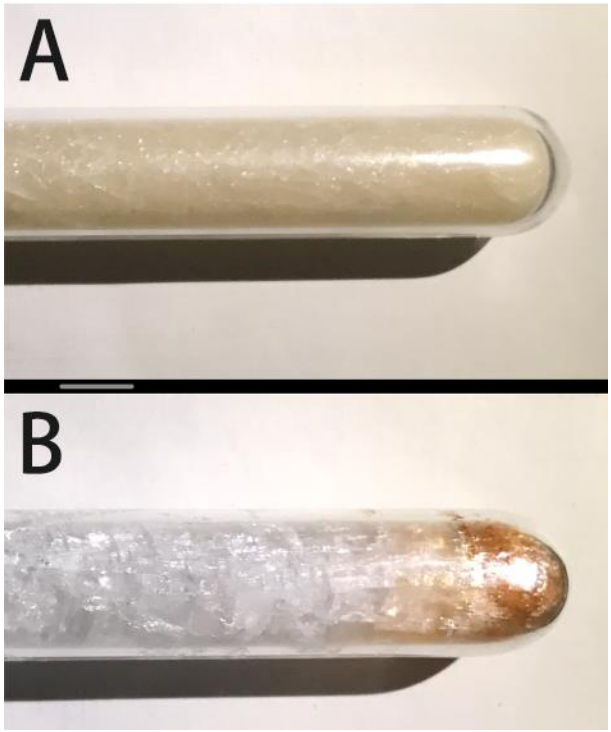


Figure 4. (**A**) Before zone melting and (**B**) after zone melting.

3.1. Influence of Zone Travel Rate on Zone Melting Purification Process

Figure 5 shows the influence of the zone travel rate on product purity. When v = 12 mm/h, v = 18 mm/h, and v = 24 mm/h, the distribution of sample purity along the axial direction was investigated. After one pass, when the zone travel rate was 12 mm/h, the product purity of samples with normalized distances of 0 to 0.6 was over 98%, and the highest purity reached 98.6%, which was over one percentage point higher than that of the initial materials. From Figure 6, it can be seen that all impurity concentrations in the fluorene increased from the beginning to the end. It can be seen in Figure 6 that the smaller the zone travel rate, the higher the purity of the product at the front end of the sample bar. When the zone travel rate (v) = 12 mm/h, the purity of the product in the front section of the sample bar was higher than when v = 18 mm/h and v = 24 mm/h. This was because the lower zone travel rate meant that the impurity mixing in the melting zone was more uniform. The impurity could transfer sufficiently between the melting zone and the crystal surface, which was more conducive to the balance of the impurity distribution between the crystal surface and the melting zone. At the same time, the time required to complete the zone melting process also increased. When the zone travel rate is small enough, the effective distribution coefficient (k_e) of the impurities will be close to the equilibrium distribution coefficient (k_0) of the impurities. However, if the zone travel rate is too small, the time cost will be greatly increased and the working efficiency will be greatly reduced. Therefore, a moderate zone travel rate should be selected to balance the purification effect and the time cost.

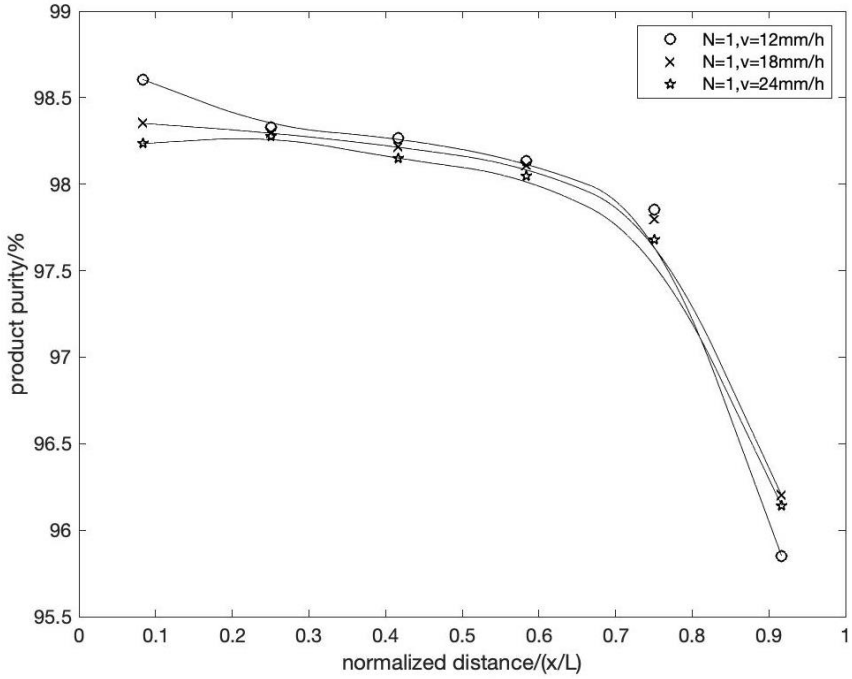


Figure 5. Influence of zone travel rate on product purity. Experimental conditions: melting temperature, 150 °C; solidification temperature, 30 °C; zone passing number, N = 1; dimensionless zone length, Z = 0.13.

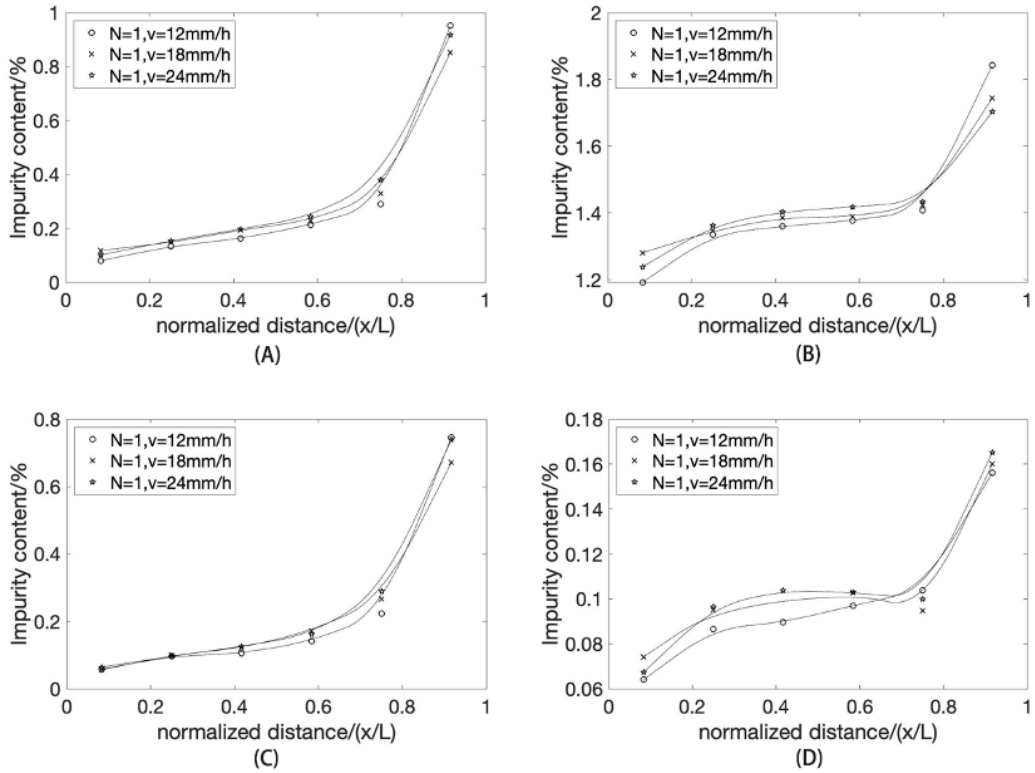


Figure 6. Effect of zone travel rate on impurity concentration. (**A**) 2-methylbiphenyl; (**B**) 4-methylbiphenyl; (**C**) 4-methyldibenzofuran; (**D**) dibenzofuran. Experimental conditions: melting temperature, 150 °C; solidification temperature, 30 °C; zone passing number, N = 1; dimensionless zone length, Z = 0.13.

3.2. Influence of Zone Length on Zone Melting Purification Process

Figures 7 and 8 show the results of the zone melting purification experiment when the lengths of the zone were 0.13 and 0.27. It can be clearly seen that the zone length of 0.27 could obtain a better purification effect when the zone passing number was one, and the highest purity reached 98.5%. When the zone length was 0.13, the highest purity was 98.3%. It can be clearly seen in Figure 7 that during the zone refining process, more impurities could be enriched in the tail when the zone length of 0.27 was used than when the zone length of 0.13 was used. Many scholars have conducted more detailed research on how large the length of the zone is [45–47]. On one hand, a large melting zone means that it can absorb more impurities. Under the same effective distribution coefficient, the ability to remove impurities is greater, which is conducive to a purification effect. On the other hand, a large melting zone will reduce the final purity of a sample due to more mixing at the impure end, which is not conducive to a purification effect. In several previous zone melting processes, the comprehensive effect of a large melting zone was favorable for a purification effect. With an increase in the zone passing number, the situation gradually reversed, and the small melting zone began to benefit the zone melting process. With an increase in the zone passing number, more and more impurities accumulated at the tail end of the sample bar, and the influence of the impurities at the tail end on the purity of the product became stronger and stronger. Therefore, it is better to use a larger melting zone for one pass. For multiple zone melting processes, a small zone length can produce a better purification effect with the zone passing number increasing. It is better to use a variable zone length in the zone melting process; that is, the first zone melting process uses a larger zone length, and the zone length gradually decreases with each additional zone melting process.

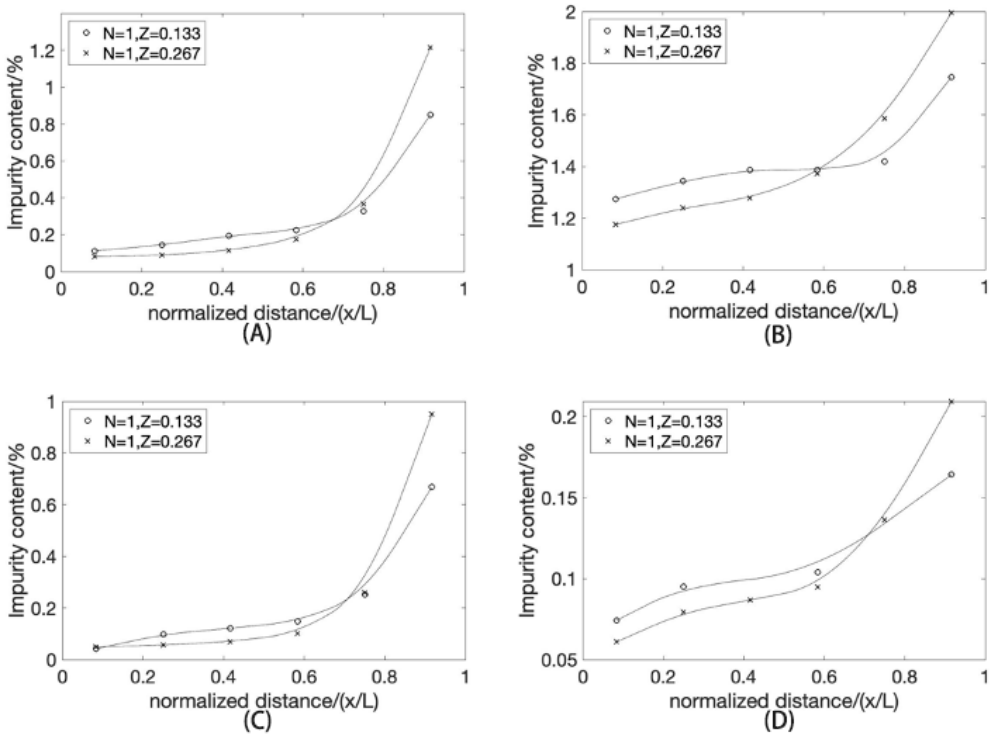


Figure 7. Effect of zone length on impurity concentration. (**A**) 2-methylbiphenyl; (**B**) 4-methylbiphenyl; (**C**) 4-methyldibenzofuran; (**D**) dibenzofuran. Experimental conditions: melting temperature, 150 °C; solidification temperature, 30 °C; zone passing number, N = 1; zone travel rate, v = 18 mm·h^{-1}.

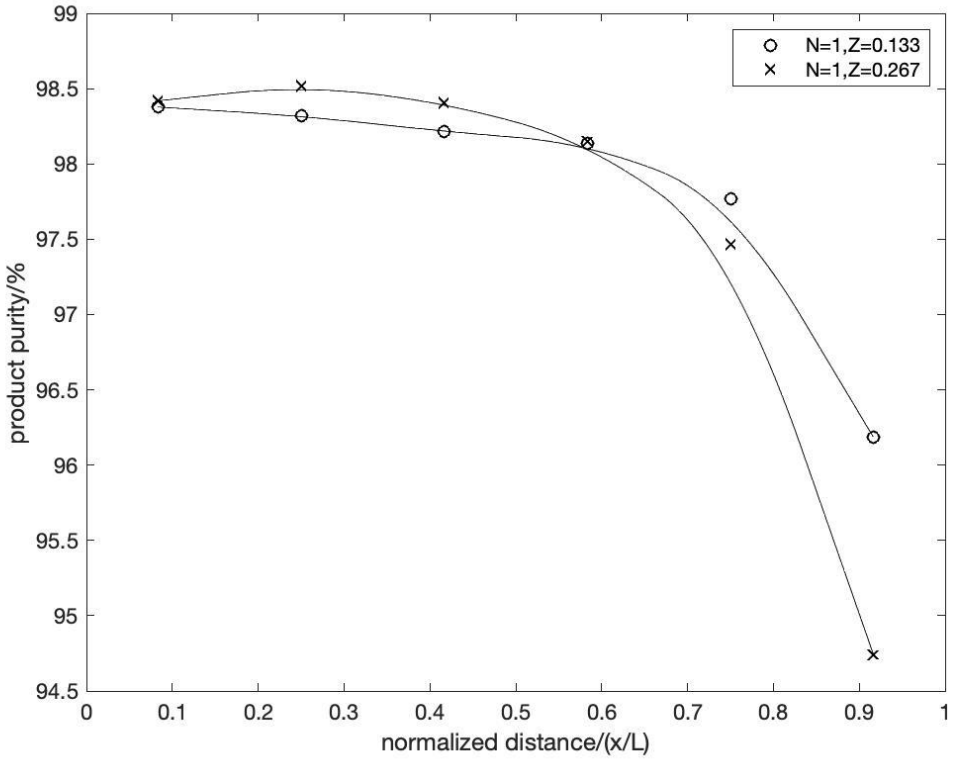


Figure 8. Effect of zone length on product purity. Experimental conditions: melting temperature, 150 °C; solidification temperature, 30 °C; zone passing number, N = 1; zone travel rate, v = 18 mm·h^{-1}.

3.3. Influence of Zone Passing Number on Zone Melting Purification Process

Figure 9 shows the product purity curves of different zone passing numbers at a zone travel rate of 18 mm/h. The abscissa is the dimensionless length of the sample bar, "0" is the starting point of the melting zone, and "1" is the ending point of the melting zone. The ordinate is the purity of the product. It can be seen from the figure that with an increase in the zone passing number, the purification effect was obviously improved. When the zone passing number was four, at the position of a dimensionless distance of the sample of 0–0.5, the purity of the product reached more than 98.7%, and the highest purity reached 99.01%, which was nearly 1.5 percentage points higher than that of the initial material. For the product with the dimensionless length x/L = 0–0.5, the average increase in the sample purity was 0.18% when N = 2 was compared with N = 1, the average increase in the sample purity was 0.32% when N = 4 was compared with N = 2, and the average increase in the sample purity was 0.5% when N = 4 was compared with N = 1. The purity of the front section of the bar was always higher than the purity of the rear section of the bar after the melting zone passes. This was because, according to Pfann's zone melting principle [48], if there is an impurity with a distribution coefficient of $k_e < 1$ in the sample, during the zone melting process, on the crystallization interface, the content of the impurity in the crystallized crystal will decrease compared to that before crystallization, and the content of this impurity in the melting zone will increase compared to that before crystallization. As the melting zone moves from "0" to "1", an impurity with a distribution coefficient of $k_e < 1$ will move from "0" to "1", and it will gather at the "1". Similarly, for impurities with a distribution coefficient of $k_e > 1$, on the crystal interface, the impurity content in the crystallized crystals will be higher than that in the melting zone. With the movement of the melting zone, impurities with a distribution coefficient of $k_e > 1$ will move from "1" to "0" and will accumulate at "0". It can be seen in Figure 10 that all impurities moved from "0" to "1". It shows that the impurity distribution coefficients in the fluorene were all less than 1.

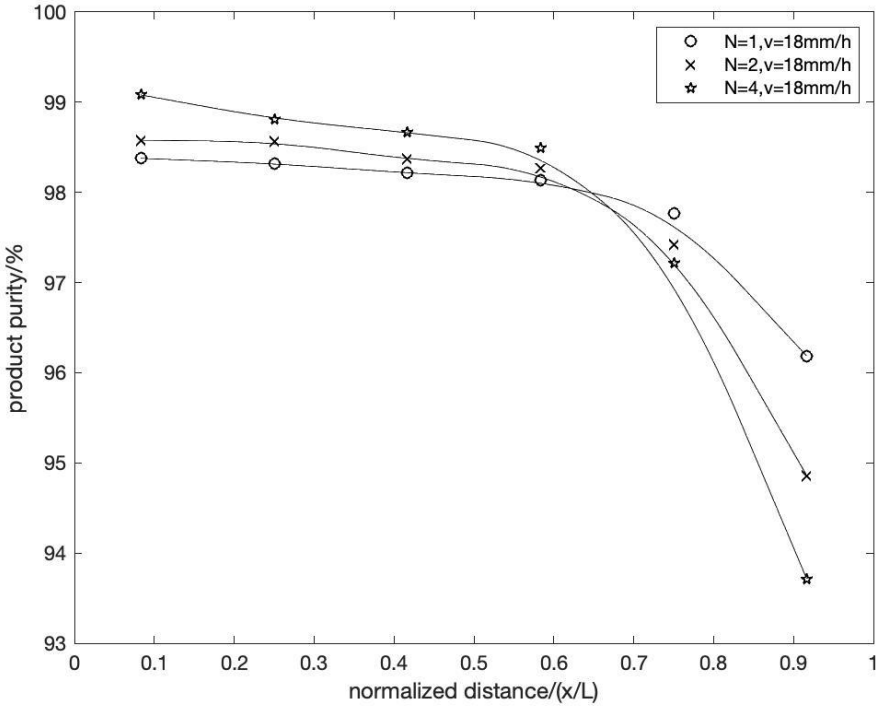


Figure 9. Effect of zone passing number on product purity. Experimental conditions: melting temperature, 150 °C; solidification temperature, 30 °C; dimensionless zone length, Z = 0.13; zone travel rate, v = 18 mm·h^{-1}.

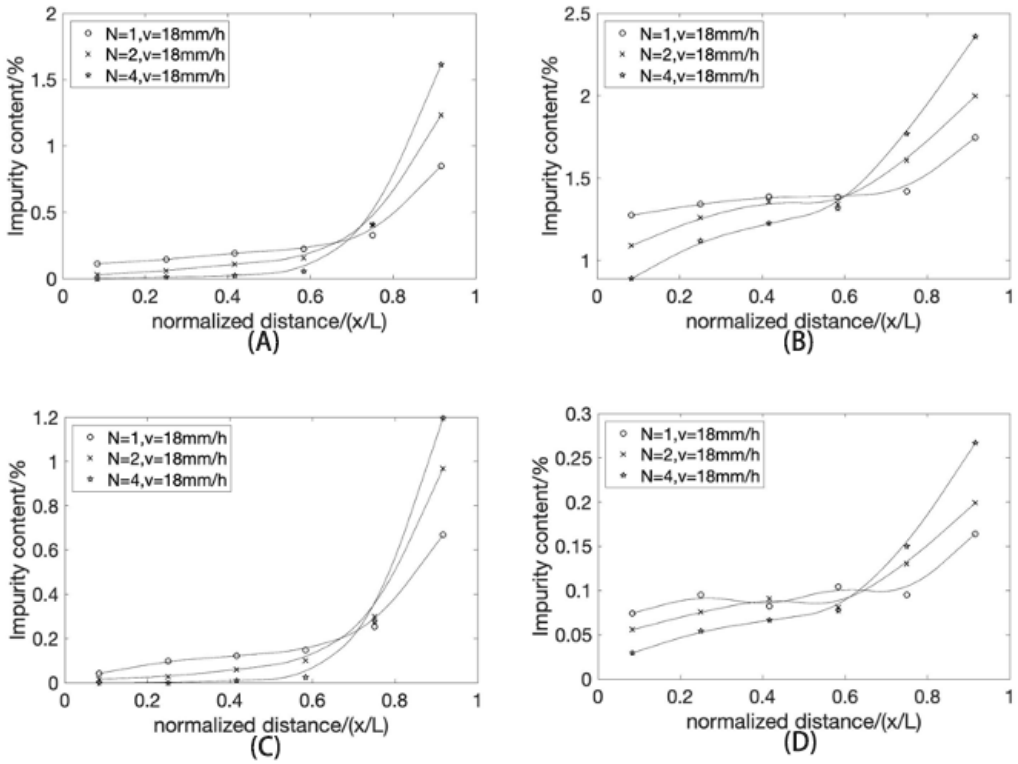


Figure 10. Effect of zone passing number on impurity concentration. (**A**) 2-methylbiphenyl; (**B**) 4-methylbiphenyl; (**C**) 4-methyldibenzofuran; (**D**) dibenzofuran. Experimental conditions: melting temperature, 150 °C; solidification temperature, 30 °C; dimensionless zone length, Z = 0.13; zone travel rate, v = 18 mm·h^{-1}.

3.4. Influence of Zone Temperature Difference on Zone Melting Purification Process

Figure 11 shows the product purity curves of different zone temperature differences. The zone temperature differences indicate the temperature differences between the melt zone and the cooler. At the position where the normalized distance of the sample was 0.1–0.8, the purity of the product when the zone temperature difference was 120 °C was better than that when the zone temperature difference was 110 °C, and the highest purity difference was 0.4% when the normalized distance was 0.6. It can be seen in Figure 12 that under the experimental conditions, the impurities 2-Methylbiphenyl, 4-Methylbiphenyl, 4-Methyldibenzofuran, and Dibenzofuran were enriched and finally accumulated at the end of the sample bar. With an increase in the zone temperature difference, more impurities were enriched at the end, and the concentration differences of the impurities between the beginning and the end increased. A better product purification effect could be obtained. The zone temperature difference is an important parameter in the zone melting purification process. On one hand, a larger zone temperature difference between the melt zone and the cooler is more conducive to the movement of molecules in the melt zone and produces less mass transfer resistance between the crystalline interface and the melt zone. On the other hand, a larger zone temperature difference means a smaller probability of structural low-temperature cooling and a higher purity of the product obtained. As shown in Figure 12, the purity of the product in the front section of the sample bar increased when the temperature difference increased, which indicates that within the range of ΔT = 110~120 °C, a larger temperature difference is conducive to the purification of fluorene, so it is appropriate to adopt a temperature difference of 120 °C.

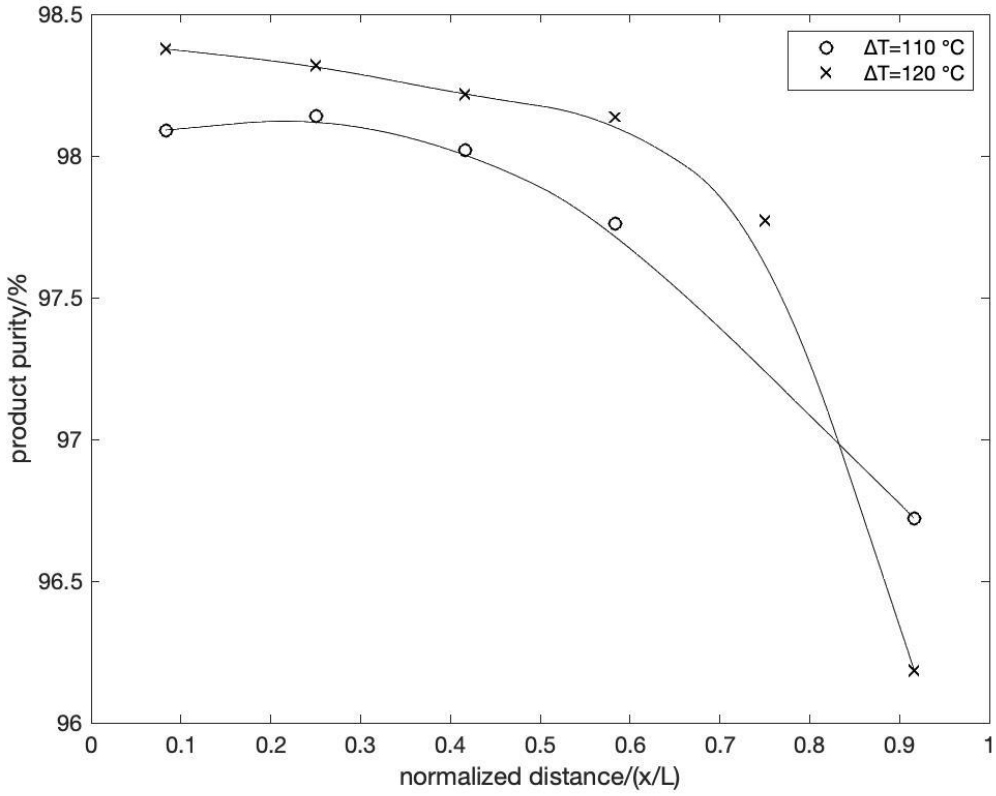


Figure 11. Effect of zone temperature difference on product purity. Experimental conditions: dimensionless zone length, Z = 0.13; zone passing number, N = 1; zone travel rate, v = 18 mm·h^{-1}.

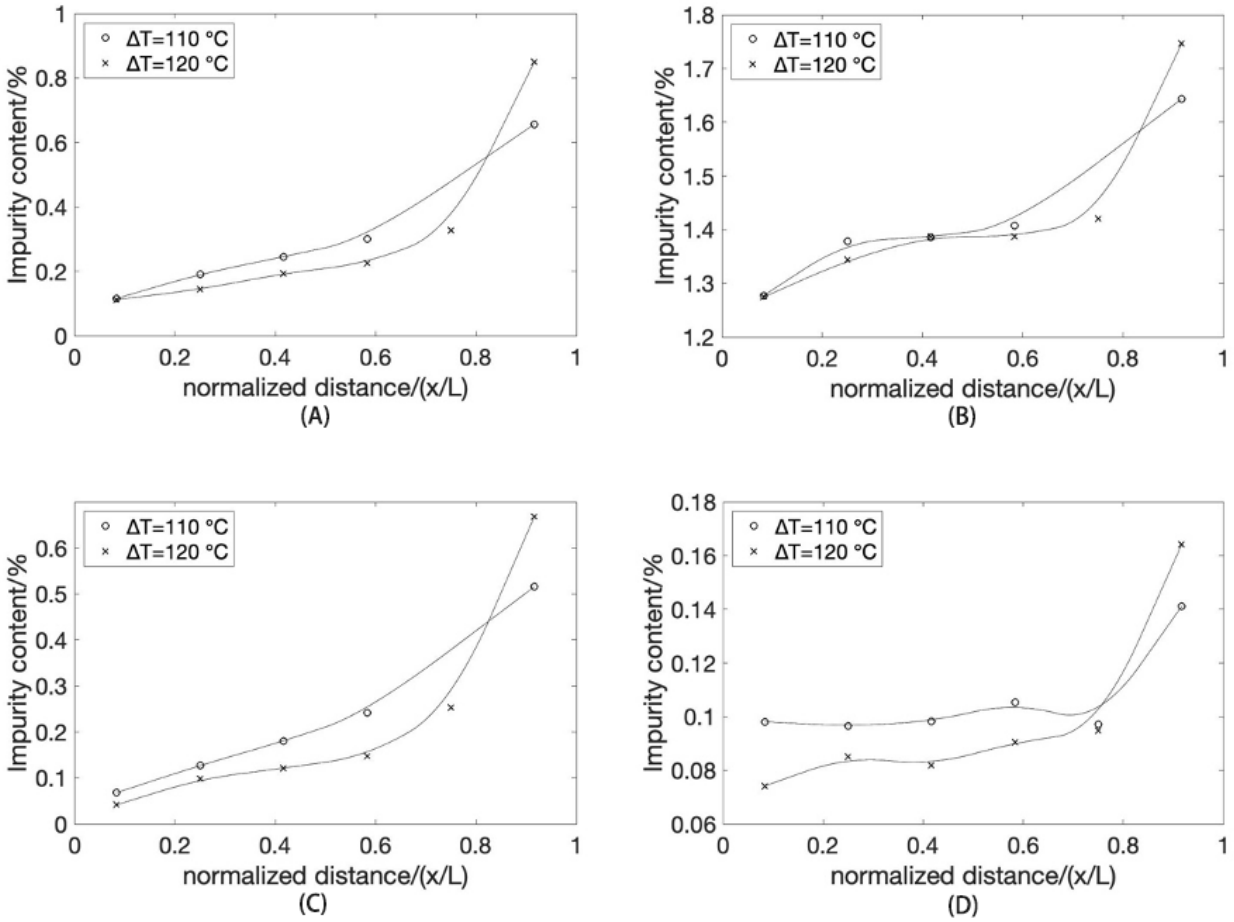


Figure 12. Effect of zone temperature difference on impurity concentration. (**A**) 2-methylbiphenyl; (**B**) 4-methylbiphenyl; (**C**) 4-methyldibenzofuran; (**D**) dibenzofuran. Experimental conditions: dimensionless zone length, Z = 0.13; zone passing number, N = 1; zone travel rate, v = 18 mm·h^{-1}.

4. Calculation of Impurity Distribution Coefficient

4.1. Model of One-Pass Zone Refining

Scholars from various countries have conducted a lot of research on the zone melting process. Lord and Reiss [49,50] established a semi-infinite mathematical model to predict the distribution of impurities along the moving direction of a melting zone after any number of zone passes, but they did not consider the impact of impurities accumulated at the end on the entire impurity distribution. On this basis, Ghosh and Spim [40,51] established a relatively complete mathematical model of the zone melting process. They considered the impact of impurities accumulated at the end on the entire impurity distribution. Based on the ideas of Ghosh and Spim, this article generalizes their model and applies it to the zone melting process of fluorene.

Before establishing a model of one pass, the following assumptions are made for the zone melting purification process:

1. The crystalline interface is in equilibrium;
2. The crystalline interface is flat.

In order to establish the zone melting purification model, Figures 13 and 14 are model diagrams of the zone melting process. The moving direction of the melting zone is defined as the direction in which the dimensionless distance (x) of the sample increases; that is, x = 0 is the starting end and x = 1 is the tail end.

- Region 1: $0 < x < 1 - z$

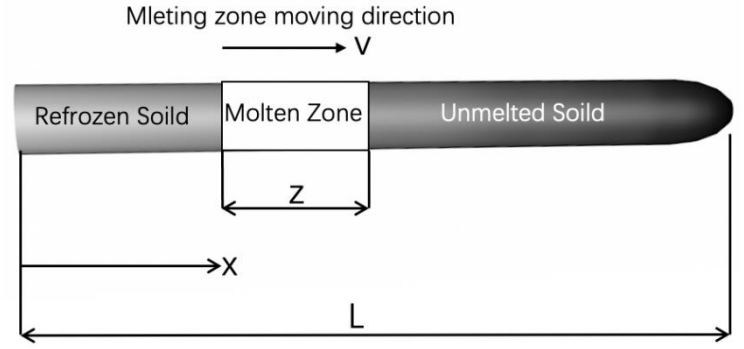


Figure 13. Model diagram of the zone melting process.

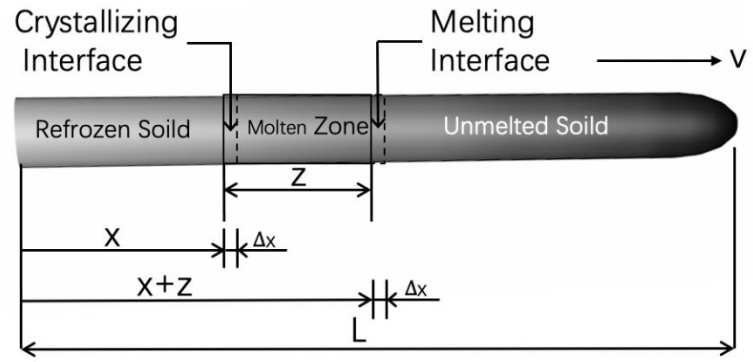


Figure 14. Model diagram of the zone melting process.

Assuming that the impurity concentration in the melt zone is I, then the change in the impurity concentration in the melt zone during the zone moving (dx) is dI.

$$dI = (C_0 - C_S)dx \tag{2}$$

$$C_S = k_e C_0 \tag{3}$$

$$C_L = I/z \tag{4}$$

$$C_0 = I_0/z \tag{5}$$

$$\int_0^x dx = \int_{I_0}^{I} \frac{dI}{C_0 - k_e I/z} \tag{6}$$

According to Formula (6), the impurity concentration distribution in region 1 after one pass can be calculated using Formula (7).

$$C_1(x)/C_0 = 1 - (1 - k_e)exp(-k_e x/z) \tag{7}$$

- Region 2: $1 - z < x < 1$

Within a unit of time, the amount of crystal produced by directional crystallization is $\rho A dx$, where ρ is the density of the material, and the density of the solid and liquid phases is assumed to be equal. A is the cross-sectional area perpendicular to the travel direction. Then, within a unit of time, the amount of crystals produced by directional crystallization accounts for a fraction of the liquid at this time, as shown in Formula (8).

$$\rho A dx/[\rho A(1 - x)] = dx/(1 - x) \tag{8}$$

The amount of crystals produced by directional crystallization accounts for a fraction of the liquid at this time, which can be expressed as $dw_l/(w_0 - w_s)$. w_l is the liquid mass; w_s is the crystal mass. Then, Formula (8) can be written as Formula (9).

$$\int_0^x \frac{dx}{1-x} = \int_{w_0}^{w_l} \frac{dw_l}{w_0 - w_s} \tag{9}$$

Then, the directional crystallization equation can be written as Formula (10).

$$w_s/w_0 = k_e(1-x)^{k_e-1} \tag{10}$$

Formula (10) can be written as Formula (11).

$$C_S(x)/C_0 = k_e(1-x)^{k_e-1} \tag{11}$$

According to the directional crystallization equation, for one pass, the impurity distribution in the last melting zone can be expressed as Formula (12).

$$C(y)/C_0' = k_e(1-y)^{k_e-1} \tag{12}$$

C_0' is the average concentration of impurities in the last melting zone after one pass is completed.

$$y = [x - (1-z)]/z \tag{13}$$

According to Formulas (12) and (13), we can obtain the following formulas:

$$\frac{C(y)}{C_0'} = k_e\left[1 - \frac{x-(1-z)}{z}\right]^{k_e-1} \tag{14}$$

$$C_0' = \left[C_0 - \int_0^{1-z} C(x)dx\right]/z \tag{15}$$

$$C(x)/C_0 = 1 - (1-k_e)exp(-k_e x/z) \tag{16}$$

According to Formulas (13)–(16), the concentration distribution of the impurities in region 2 after one pass can be obtained.

$$C_1(x)/C_0 = \{1 - (1-k_e)exp[-k_e(1-z)/z]\} \times \{1 - [x-(1-z)]/z\}^{k_e-1} \tag{17}$$

After one pass, all impurity concentration formulas were imported into mathematical software, and the effective distribution coefficient (k_e) corresponding to the travel rate of one pass was obtained using the least square method.

- Calculation of equilibrium distribution coefficient

According to the research by Kurz and Fisher [52], the relationship between k_e and k_0 can be expressed using the following formula:

$$k_e = \frac{k_0}{k_0 + (1-k_0)exp(-v\delta/D)} \tag{18}$$

where k_e is the effective distribution coefficient and k_0 is the equilibrium distribution coefficient. v is the travel rate of the zone. δ is the thickness of the diffusion boundary layer, and D is the diffusion coefficient of the impurities in the melt zone.

Formula (18) can be transformed into the following formulas:

$$ln\left(\frac{1}{k_e} - 1\right) = ln\left(\frac{1}{k_0} - 1\right) - \frac{v\delta}{D}\ for\ k_0 < 1 \tag{19}$$

$$ln\left(1-\frac{1}{k_e}\right)=ln\left(1-\frac{1}{k_0}\right)-\frac{v\delta}{D}\ for\ k_0>1 \tag{20}$$

A linear regression was performed on $ln\left(\frac{1}{k_e}-1\right)$ or $ln\left(1-\frac{1}{k_e}\right)$ and the zone travel rate (v), and the equilibrium distribution coefficient (k_0) could be calculated from the intercept of the linear regression equation.

4.2. Impurity Distribution Coefficient

Table 2 shows the k_e and k_0 values of all impurities. The k_e values of all impurities were obtained via mathematical software fitting when the zone travel rates were 12 mm·h^{-1}, 18 mm·h^{-1}, and 24 mm·h^{-1}. Then, all k_e values and rates were linearly fitted using the least squares method. Then, the k_0 values of all impurities were obtained using the linear equation intercepts. The k_0 values of 2-Methylbiphenyl, 4-Methylbiphenyl, 4-Methyldibenzofuran, and dibenzofuran were 0.2441, 0.5850, 0.2377, and 0.3497, respectively. These four impurity concentrations accounted for more than 85% of the total impurity concentration in the initial fluorene. Therefore, after the zone melting purification process, the main impurities in the initial fluorene will be enriched in the end, and a purified product will be obtained in the beginning region.

Table 2. Effective and equilibrium distribution coefficients of different impurities.

Effective and Equilibrium Distribution Coefficients of Different Impurities						
	Impurity	k_e			k_0	R^2
		v = 12 mm·h^{-1}	v = 18 mm·h^{-1}	v = 24 mm·h^{-1}		
D	2-Methylbiphenyl	0.2757	0.2971	0.3110	0.2441	0.9828
E	4-Methylbiphenyl	0.6577	0.7150	0.7300	0.5850	0.9048
F	4-Methyldibenzofuran	0.2602	0.2710	0.2837	0.2377	0.9985
G	Dibenzofunan	0.4090	0.4557	0.4756	0.3497	0.9473

5. Conclusions

According to the experimental results, it can be seen that zone melting purification technology is effective for the purification of fluorene. The purification effect of fluorene can be improved by using a larger zone length in the initial zone melting purification process, a smaller zone travel rate in the whole zone melting purification process, multiple zone melting purification processes, and a larger zone temperature difference. Based on the experimental conditions, the k_0 values of the impurities 2-Methylbiphenyl, 4-Methylbiphenyl, 4-Methyldibenzofuran, and Dibenzofunan were 0.2441, 0.5850, 0.2377, and 0.3497, respectively, and the k_0 values of all impurities were less than 1. For the impurities 2-Methylbiphenyl, 4-Methyldibenzofuran, and dibenzofuran, in particular, the equilibrium distribution coefficients (k_0) were much less than 1. Based on the experimental conditions, after four zone melting purification processes, the purity of the product at the position of a normalized distance of 0-0.5 of the sample exceeded 98.7%, and the highest purity reached 99.01%, which was nearly 1.5% higher than that of the initial fluorene. Zone melting purification technology provides a new idea for the preparation of high-purity fluorene and is completely feasible. Compared to the solution crystallization method, this technology has the advantages of low energy consumption, environmental friendliness, and no need for solvents. It is more in line with the requirements of the new purification technology in today's world, and it has broad prospects for industrial application. However, at present, this purification technology has the problem of low purification efficiency, as it is time-consuming. If it is used in industrialization, it obviously has no economic advantage. Therefore, in order to better meet the requirements of industrialization, how to improve the purification efficiency of this technology needs further research (such as increasing the number of melting zones, developing special equipment, etc.).

Author Contributions: Conceptualization, Y.S.; Methodology, Y.S.; Software, Y.S.; Validation, Y.S.; Formal analysis, Y.S.; Investigation, Y.S.; Resources, Y.S.; Data curation, Y.S.; Writing—original draft, Y.S.; Writing—review & editing, M.C.; Supervision, J.L.; Funding acquisition, J.L. All authors have read and agreed to the published version of the manuscript.

Funding: This research received no external funding.

Data Availability Statement: Data available on request due to restrictions eg privacy or ethical. The data presented in this study are available on request from the corresponding author. The data are not publicly available due to laboratory rules.

Conflicts of Interest: The authors declare no conflict of interest.

Glossary

A	Cross-sectional area perpendicular to the travel direction, m^2
C_S	Impurity concentration in solid phase, $mg \cdot g^{-1}$
C_L	Impurity concentration in liquid phase, $mg \cdot g^{-1}$
C_0	Initial impurity concentration of the sample, $mg \cdot g^{-1}$
k_e	Effective distribution coefficient of impurities
k_0	Equilibrium distribution coefficient of impurities
I	The total amount of a certain impurity in the melting zone, mg
I_0	The initial total amount of a certain impurity in the melting zone, mg
L	Sample length
x	Dimensionless distance from the starting point
D	Diffusion coefficient of impurity in melt zone
Z	Dimensionless zone length
d	Thickness of diffusion boundary layer, mm
N	Zone passing number

References

1. Wei, H. Method for Purifying Refined Fluorene by Crystallizing Process. CN101182278, 21 May 2008.
2. Xiong, D. New Process for Purifying and Refining Coarse Fluorene. CN103304365A, 18 September 2013.
3. E, Y.; He, F.; Xu, H.; Li, S.; Liu, T.; Cui, S. Process for Purifying Industrial Fluorene. CN102807466A, 5 December 2012.
4. Yin, Q.; Li, H.; Yang, L.; Hou, B.; Wang, Z.; Zhang, M.; Wang, J.; He, Y. Crystallization Method for Fluorene Purification. CN103224441A, 31 July 2013.
5. Wei, F.; Luo, G. Method for Purifying Industrial Fluorine with Drum. Crystallization Method for Fluorene Purification. CN105523878A, 27 April 2016.
6. Pfann, W.G. Techniques of Zone Melting and Crystal Growing. *Solid State Phys.* **1957**, *4*, 423–521.
7. Kousaka, Y.; Iwasaki, S.; Sayo, T.; Tanida, H.; Matsumura, T.; Araki, S.; Akimitsu, J.; Togawa, Y. Chirality-controlled enantiopure crystal growth of a transition metal monosilicide by a floating zone method. *Jpn. J. Appl. Phys.* **2022**, *61*, 045501. [CrossRef]
8. Kantuptim, P.; Kato, T.; Nakauchi, D.; Kawaguchi, N.; Watanabe, K.; Yanagida, T. Optical and Scintillation Characteristics of Tb-doped $La_2Si_2O_7$ Single Crystal. *Sens. Mater.* **2023**, *35*, 451–458. [CrossRef]
9. Ichiba, K.; Takebuchi, Y.; Kimura, H.; Kato, T.; Nakauchi, D.; Kawaguchi, N.; Yanagida, T. Analysis of Photoluminescence and Dosimetric Properties of (Ce, Tb)-codoped Magnesium Orthosilicate Single Crystals. *Sens. Mater.* **2023**, *35*, 475–481. [CrossRef]
10. Huang, D.; Xiao, T.; Fu, B.; Xu, S.; Huang, Y.; Deng, W.; Zhou, Z. Up-Conversion Photoluminescence in Thulia and Ytterbia Co-Doped Yttria-Stabilized Zirconia Single Crystals. *Crystals* **2023**, *13*, 460. [CrossRef]
11. Fukushima, H.; Nakauchi, D.; Kato, T.; Kawaguchi, N.; Yanagida, T. Photoluminescence and Scintillation Properties of Ce-doped $(Mg_xCa_{1-x})HfO_3$ Single Crystals. *Sens. Mater.* **2023**, *35*, 429–437. [CrossRef]
12. Chen, L.-D.; Shu, L.-H.; Zhang, B.H.; Liu, L.; Lei, L.; Shao, Y.; Huang, F.-Z.; Lv, Y.-Y.; Cheng, Z.-X.; Wang, J.-L.; et al. Significant magneto-dielectric effect in SrNd2Fe2O7 at room temperature. *Appl. Phys. Lett.* **2023**, *122*, 072903. [CrossRef]
13. Boatner, L.A.; Finch, C.B.; Brundage, W.E.; Kolopus, J.A.; Gruzalski, G.R.; Johanns, K.E.; Sudharshan Phani, P.; Pharr, G.M.; Oliver, W.C. Synthesis and characterization of metal carbides for nanoindentation tip applications. *J. Appl. Phys.* **2023**, *133*, 095107. [CrossRef]
14. Bauer, A.; Benka, G.; Neubauer, A.; Regnat, A.; Engelhardt, A.; Resch, C.; Wurmehl, S.; Blum, C.G.F.; Adams, T.; Chacon, A.; et al. Compositional Studies of Metals with Complex Order by means of the Optical Floating-Zone Technique. *Phys. Status Solidi B-Basic Solid State Phys.* **2022**, *259*, 2100159. [CrossRef]
15. Wu, T.; Zhang, Q.; Shi, Y.; Wang, L.; Xiong, Y.; Wang, H.; Fang, J.; Ni, J.; He, H.; Zhou, Z.; et al. Eu^{3+}-Doped (Gd, La)AlO_3 Perovskite Single Crystals: Growth and Red-Emitting Luminescence. *Materials* **2023**, *16*, 488. [CrossRef]

16. Upatov, M.; Vleugels, J.; Koval, Y.; Bolbut, V.; Bogomol, I. Microstructure and mechanical properties of B_4C-NbB_2-SiC ternary eutectic composites by a crucible-free zone melting method. *J. Eur. Ceram. Soc.* **2021**, *41*, 1189–1196. [CrossRef]
17. Su, H.; Jiang, H.; Zhang, Z.; Zhao, D.; Liu, Y.; Shen, Z.; Guo, Y.; Yang, C.; Ren, W. Crucible-free fabrication of ZrB_2-SiC composite ceramics with ultra-fine eutectic microstructure by laser surface zone-melting: The selection of lasers. *Ceram. Int.* **2023**, *49*, 9346–9354. [CrossRef]
18. Sturm, F.; Trempa, M.; Schuster, G.; Gotz, P.; Wagner, R.; Barroso, G.; Meisner, P.; Reimann, C.; Friedrich, J. Material evaluation for engineering a novel crucible setup for the growth of oxygen free czochralski silicon crystals. *J. Cryst. Growth* **2022**, *584*, 126582. [CrossRef]
19. Okazaki, K.; Nakauchi, D.; Fukushima, H.; Kato, T.; Kawaguchi, N.; Yanagida, T. Radiation-induced Luminescence Properties of Tm-doped $Bi_4Ge_3O_{12}$ Single Crystals. *Sens. Mater.* **2023**, *35*, 459–466. [CrossRef]
20. Nanda, N.; Soni, P.H. Growth and characterization of $InBi_{0.95}Te_{0.05}$ and $InBi_{0.9}0Te_{0.10}$ crystals. *Opt. Mater.* **2023**, *136*, 113430. [CrossRef]
21. Jin, M.; Lu, X.; Guo, L.; He, F.; Bai, X.; Li, R.; Lin, S. Thermoelectric properties of ductile $Ag_2S_{0.7}Te_{0.3}$ prepared via zone melting method. *Solid State Commun.* **2023**, *364*, 115123. [CrossRef]
22. Islam, A.; Aynul, A.T. Erbium Related Photoluminescence of Silicon: Influence of Co-doping with Oxygen and Hydrogenation. In Proceedings of the 7th International Conference on Advanced Engineering and Technology (ICAET), Incheon, Republic of Korea, 18–20 December 2020.
23. Denisenko, D.S.; Timonina, A.V.; Fursova, T.N.; Kolesnikov, N.N. Cr^{2+} distribution in ZnSe crystals grown from melt. *J. Cryst. Growth* **2023**, *603*, 127037. [CrossRef]
24. Bhandari, S.; Zvanut, M.E. Fe-related optical transitions in floating zone and Czochralski grown beta-Ga_2O_3 crystals. *J. Appl. Phys.* **2021**, *130*, 165701. [CrossRef]
25. Yu, C.; Pan, B.; Wang, Z.; Chen, D.; Zhang, X.; Yang, W.; Zhang, D.; Lu, W. Research of High-Purity Lanthanum Prepared by Zone Refining. *Materials* **2022**, *15*, 4603. [CrossRef]
26. Cheung, N.; Bertazzoli, R.; Garcia, A. Experimental impurity segregation and numerical analysis based on variable solute distribution coefficients during multi-pass zone refining of aluminum. *J. Cryst. Growth* **2008**, *310*, 1274–1280. [CrossRef]
27. Nakamura, M.; Watanabe, M.; Tanaka, K.; Kirihata, A.; Sumomogi, T.; Hoshikawa, H.; Tanaka, I. Zone Refining of Aluminum and Its Simulation. *Mater. Trans.* **2014**, *55*, 664–670. [CrossRef]
28. Hashimoto, E.; Ueda, Y. Zone Refining of High-Purity Aluminum. *Mater. Trans. JIM* **1994**, *35*, 262–265. [CrossRef]
29. Wan, H.; Zhao, J.; Yang, B.; Xu, B.; Duan, M.; Kong, L.; Dai, Y. Study on the effective distribution coefficient of impurity separation in the preparation of high purity aluminum. *J. Mater. Res. Technol.-JmrT* **2020**, *9*, 10366–10376. [CrossRef]
30. Wan, H.; Xu, B.; Yang, B.; Duan, M.; Yang, J.; Dai, Y.; Kong, L.; Li, Y. Effect of Silicon Separation on the Preparation of High-Purity Aluminum. *Silicon* **2021**, *13*, 399–407. [CrossRef]
31. Ma, Y.; Yasuda, K.; Ido, A.; Shimao, T.; Zhong, M.; Hagiwara, R.; Nohira, T. Silicon Refining by Solidification from Liquid Si-Zn Alloy and Floating Zone Method. *Mater. Trans.* **2021**, *62*, 403–411. [CrossRef]
32. Kozhevnikov, O.E.; Pylypenko, M.M.; Kozhevnikova, M.F. Zone Recrystallization of Zirconium and Hafnium. *East Eur. J. Phys.* **2021**, *1*, 55–62. [CrossRef]
33. He, B.; Wang, W.; Jiang, W.; Xu, B.; Yang, H. Removing of Fe, Pb and Hg from Crude Selenium by Fractional Crystallization. *Metals* **2023**, *13*, 739. [CrossRef]
34. Roumié, M.; Zahraman, K.; Zaiour, A.; Mohanna, Y.; Hage-Ali, M. Study of segregation process of impurities in molten tellurium after one pass of three conjoint zones in zone refining. *J. Cryst. Growth* **2006**, *289*, 260–268. [CrossRef]
35. Shim, M.; Kim, Y.M.; Lee, H.H.; Hong, S.J.; Lee, J.H. Separation behavior of impurities and selenium reduction by the reactive zone refining process using high-frequency induction heating to purify Te. *J. Cryst. Growth* **2016**, *455*, 6–12. [CrossRef]
36. Liu, Y.C.; Moss, R.; Dost, S. A computational thermal analysis for the zone-refining processes of Cd and Te. *J. Cryst. Growth* **2006**, *293*, 146–156. [CrossRef]
37. Prasad, D.S.; Munirathnam, N.R.; Rao, J.V.; Prakash, T.L. Effect of multi-pass, zone length and translation rate on impurity segregation during zone refining of tellurium. *Mater. Lett.* **2006**, *60*, 1875–1879. [CrossRef]
38. Yang, G.; Govani, J.; Mei, H.; Guan, Y.; Wang, G.; Huang, M.; Mei, D. Investigation of influential factors on the purification of zone- refined germanium ingot. *Cryst. Res. Technol.* **2014**, *49*, 269–275. [CrossRef]
39. Wang, S.; Fang, H.S.; Jin, Z.L.; Zhao, C.J.; Zheng, L.L. Integrated analysis and design optimization of germanium purification process using zone-refining technique. *J. Cryst. Growth* **2014**, *408*, 42–48. [CrossRef]
40. Spim, J.A., Jr.; Bernadou, M.J.S.; Garcia, A. Numerical modeling and optimization of zone refining. *J. Alloys Compd.* **2000**, *298*, 299–305. [CrossRef]
41. Ganschow, S.; Klimm, D.; Bertram, R. On the effect of oxygen partial pressure on the chromium distribution coefficient in melt-grown ruby crystals. *J. Cryst. Growth* **2011**, *325*, 81–84. [CrossRef]
42. Ren, Y.; Li, J.; Duan, X. Determination of Equilibrium Distribution Coefficients of Impurities in Phosphorus by Vertical Zone-melting Technique. *Chin. J. Chem. Eng.* **2011**, *19*, 223–226. [CrossRef]
43. Solà Cervera, J.L.; Keil, P.; König, A. Determination of Distribution Coefficients in 1-Ethyl-3-Methyl Imidazolium Chloride-Methylimidazole Mixtures by Zone Melting. *Chem. Eng. Technol.* **2010**, *33*, 821–826. [CrossRef]

44. Qi, Y.-B.; Li, J.; Zhou, K.; Luo, J.-H.; Jin, Y.; Wang, B.-M. Study on Segregation Process and Equilibrium Distribution Coefficients of Impurities during Zone Refining of Bibenzyl. *Sep. Sci. Technol.* **2013**, *48*, 820–826. [CrossRef]
45. Rodway, G.H.; Hunt, J.D. Optimizing zone-refining. *J. Cryst. Growth* **1989**, *97*, 680–688. [CrossRef]
46. Qi, Y.; Li, J.; Wang, B.; Zhou, K.; Luo, J.; Ye, C.; Jia, X. Numerical Modeling and Optimization of Zone Refining in High Purification of Bibenzyl. *J. Chem. Eng. Jpn.* **2012**, *45*, 571–576. [CrossRef]
47. Wilcox, W.R.; Friedenberg, R.; Back, N. Zone Melting of Organic Compounds. *Chem. Rev.* **1964**, *64*, 187–220. [CrossRef]
48. Pfann, W.G. Principles of Zone-Melting. *J. Met.* **1952**, *4*, 747–753. [CrossRef]
49. Lord, N.W. Analysis of Molten-Zone Refining. *Trans. Am. Inst. Min. Metall. Eng.* **1953**, *197*, 1531–1533.
50. Reiss, H. Mathematical Methods for Zone-Melting Processes. *Trans. Am. Inst. Min. Metall. Eng.* **1954**, *200*, 1053–1059. [CrossRef]
51. Ghosh, K.; Mani, V.N.; Dhar, S. Numerical study and experimental investigation of zone refining in ultra-high purification of gallium and its use in the growth of GaAs epitaxial layers. *J. Cryst. Growth* **2009**, *311*, 1521–1528. [CrossRef]
52. Kurz, W.; Fisher, D.J. *Fundamentals of Solidification*; Trans Tech Publications: Aedermannsdorf, Switzerland, 1984; pp. 1–353.

Disclaimer/Publisher's Note: The statements, opinions and data contained in all publications are solely those of the individual author(s) and contributor(s) and not of MDPI and/or the editor(s). MDPI and/or the editor(s) disclaim responsibility for any injury to people or property resulting from any ideas, methods, instructions or products referred to in the content.